J Mater Sci (2010) 45:2991–2994
DOI 10.1007/s10853-010-4299-5

Nanometer scale crystallographic texture mapping of platinum and lead zirconate titanate thin films by electron backscatter diffraction

G. R. Fox · X. Han · T. M. Maitland ·
M. D. Vaudin

Received: 28 October 2009 / Accepted: 3 February 2010 / Published online: 13 February 2010
© Springer Science+Business Media, LLC 2010

Abstract Automated high resolution electron backscatter diffraction was used to map the local crystallographic texture of Pt and $PbZr_{1-x}Ti_xO_3$ (PZT) thin films with a resolution as high as 5 nm. The Pt and PZT films consisted of 99.9% and 94.3% {111} textured grains (i.e., with (111) planes parallel to the substrate surface), respectively. The average Pt and PZT grain sizes were 46 ± 30 nm and 65 ± 30 nm, respectively. Quantification of misorientation distributions and the fraction of non-{111}-textured grains demonstrates the potential of this local texture measurement method for quantifying the ferroelectric variability limits of PZT-based capacitors.

G. R. Fox (✉)
Fox Materials Consulting, LLC, Colorado Springs,
CO 80908, USA
e-mail: glen_fox_pa@msn.com

X. Han · T. M. Maitland
HKL Technology, Inc, Danbury, CT 06810, USA
e-mail: xdhan@bjut.edu.cn

T. M. Maitland
e-mail: tim.maitland@fei.com

M. D. Vaudin
National Institute of Standards and Technology, Gaithersburg,
MD 20899, USA

Present Address:
X. Han
Institute of Microstructure and Property of Advanced Materials,
Beijing University of Technology, 100 Ping Le Yuan, Chaoyang
District, Beijing 100022, People's Republic of China

T. M. Maitland
FEI Company, Hillsboro, OR 97124, USA

Introduction

One of the primary questions concerning the scaling of ferroelectric random access memory (FRAM) for high density is whether the ferroelectric capacitor area can be reduced below 1 μm^2 without increasing the capacitor-to-capacitor variability of the switchable polarization, P_{sw}. This question has been addressed by applying piezo-force microscopy (PFM) techniques, but unambiguous interpretation of the results is not possible without accompanying crystallographic data [1]. A capacitor P_{sw} maximum limit is determined by the vector sum of individual ferroelectric $PbZr_{1-x}Ti_xO_3$ (PZT) grain polarizations, and this vector sum is determined by the orientations of the crystallites in the grain assemblage, i.e., the local crystallographic texture [2]. Much literature has been published on PZT thin film texture measurements by X-ray diffraction and transmission electron microscopy, but these techniques suffer from limitations of macroscopic texture measurements and texture measurements of thin cross sections, respectively [3, 4]. In order to understand the capacitor-to-capacitor variability introduced solely by the crystallographic texture, a method for measuring the local PZT texture within a capacitor and for the entire capacitor area is required. As has been demonstrated for Cu and Al metallization layers, automated electron backscatter diffraction (EBSD) is an ideal method for mapping the local texture of polycrystalline thin films [5, 6]. Few EBSD results have been published on Pt thin films; in addition to a lack of corresponding Pt film deposition conditions, the resolution of the reported EBSD measurements were limited to approximately 40 nm [7]. With a few exceptions, [8, 9] studies on EBSD texture mapping of PZT have been limited to bulk ceramic samples with grain sizes in excess of 1 μm [10]. Recent advances in EBSD resolution limits

have been achieved by the use of a thermally assisted field emission gun (FEG) scanning electron microscope that improves probe current stability and allows moderate current in a small spot size resulting in an improved diffracted intensity that is collected by an EBSD screen with increased detection area. By employing these equipment improvements, maps of the localized texture were generated from nano-grained Pt and PZT films over areas equivalent to typical FRAM capacitors. The Pt electrode layer acts as a template for PZT-textured film growth; therefore, it is of interest to quantify the localized texture of both Pt and PZT films [11]. The study not only demonstrates resolution improvements helpful to thin film analysis, but also shows that similar resolution can be achieved for both metal and insulating films.

Experimental procedure

Platinum thin films with a thickness of 100 nm were deposited by DC magnetron sputtering using an ULVAC ZX-1000 production multi-chamber tool.[1] The films were deposited onto 150-mm diameter, [100]-oriented Si substrates coated with 500 nm SiO_2 grown by plasma-enhanced chemical vapor deposition and 20 nm TiO_2 deposited by sputtering. During Pt deposition in an Ar atmosphere, the $TiO_2/SiO_2/Si$ substrate was heated to a temperature of 500 °C [9]. According to X-ray diffraction (XRD) measurements the Pt films exhibited a {111}-textured volume fraction of 1.00 and a rocking curve full-width-half-maximum of 3°. The ULVAC tool was also used to RF sputter deposit Ca, La, and Sr doped $PbZr_{0.40}Ti_{0.60}O_3$ with a thickness of 180 nm onto unheated Pt-coated substrates. After deposition, the PZT films were annealed in an Ar/O_2 atmosphere using a two-step process of which the first step was at 550 °C for 90 s, and the second step was at 725 °C for 20 s [12, 13]. XRD measurements of the PZT films confirmed that the films consisted of a bimodal texture with volume fractions of 0.95 ± 0.02 {111}-textured, 0.03 ± 0.01 {100}-textured, and 0.02 ± 0.01 randomly oriented grains [14].

Samples for EBSD evaluation were prepared by cleaving approximately 7 mm × 7 mm pieces of coated wafer and pasting them to a brass SEM stub using silver paint. The edges of the sample were carefully coated with silver paint to ensure contact to the exposed Pt film at the sample edge. By maintaining a small sample size, and ensuring a proper electrical ground with well-cured silver paint and optimized electron probe parameters, it was possible to avoid sample charging and collect EBSD patterns without coating samples with a conductive layer. It is assumed that the grounded Pt film underlying the PZT film provided sufficient conduction to avoid sample charging. Coating PZT thin films with a carbon layer allowed a broader range of electron probe parameters without sample charging, but it reduced the clarity of the EBSD patterns and was, therefore, not employed.

Automated EBSD measurements were completed by using an HKL Technology detector and software package [10] combined with a high resolution scanning electron microscope (SEM) equipped with a thermal field emission electron source. SEM operating parameters were optimized at 25 kV acceleration voltage, 5 nA beam current, 10-mm working distance, and 30 μm aperture to produce the highest quality EBSD patterns while minimizing sample drift. A matrix of EBSD patterns was collected from each sampled area, and the EBSD patterns from the Pt and PZT films (tilted at 70° from the incident electron beam) were automatically indexed according to face-centered cubic and cubic pervoskite (the 1% PZT tetragonality was ignored to simplify the automatic indexing) structures, respectively. A matrix of EBSD patterns was collected from the Pt sample by stepping the beam along the surface in increments of 5 nm at a step rate of 20 points/s. The PZT data were collected using 10-nm steps and a step rate of 10 points/s. Euler angles describing the crystal orientation were calculated from each indexed diffraction pattern to produce a data set for generating crystallographic orientation and grain boundary maps.

Results and discussion

Out of 68203 data points collected from a 1.205 × 1.415 μm area of Pt, 79.85% of the EBSD patterns could be indexed. The remaining 20.15% of points exhibited zero solutions, in many cases, due to the occurrence of low intensity or non-unique diffraction at the Pt grain boundaries. In order to complete grain boundary and orientation mapping, the zero solutions were eliminated by using a nearest-neighbor fill algorithm. Of the indexed EBSD patterns, 99.9% exhibited {111} plane orientation within 12° of the substrate surface. Because a constant step size was used for data collection, the percentage of EBSD patterns exhibiting {111} orientation is proportional to the {111}-textured sample area after zero solution reduction. The {111}-texture population and cumulative distributions shown in Fig. 1 reveal that more than 90% of the sample area has a misorientation of less than 4.0° relative to ideal {111}-texture, but the {111} population density does not converge to zero until 11.1°. A map of all {111} textured grains (gray) within the 12° distribution limit is shown in

[1] Certain commercial products are identified in the text to more accurately describe the experimental procedure. Such identification does not imply endorsement by NIST.

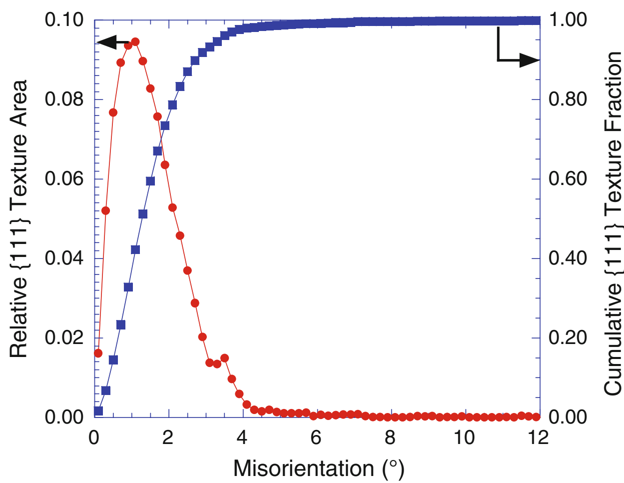

Fig. 1 Pt area distribution and Pt cumulative area distribution of {111}-textured grains with respect to misorientation angle relative to ideal {111} texture

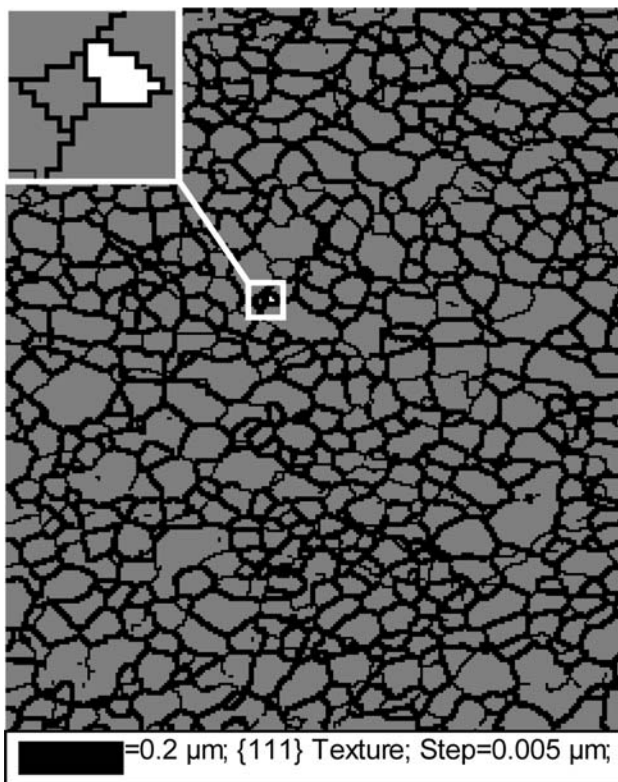

Fig. 2 Pt EBSD map of {111}-textured grains (*gray*) with a misorientation of less than 12° from ideal {111} texture. The overlapping grain boundary map shows grain misorientation of 2°–10° (*thin lines*) and greater than 10° (*thick lines*) with a population of 827 grains having an average size of 46 ± 30 nm. The inset shows a non-{111}-textured grain (white) at a 5× magnification relative to the main map

Fig. 2. In addition, a superimposed grain boundary map shows boundaries with misorientations between 2° and 10° and greater than 10°, indicated by thin and thick solid lines, respectively. The largest grain falling outside of the 12° {111} distribution limit (white) can be observed in the inset of Fig. 2. The non-{111} grains are much smaller than the majority of {111} textured grains, which exhibit an average grain size of 46 ± 30 nm (the error number being the standard deviation).

A PZT {111} texture map (Fig. 3) was generated in a manner similar to that described for Pt, from a 20295-point data matrix of which 37.66% was indexed. The higher percentage of zero solutions in comparison with Pt is a result of the lower PZT diffraction intensity and potentially increased grain boundary disorder within the relatively more complex perovskite crystal structure. Although the percentage of zero solutions for the PZT data set is more than double that observed for Pt, an average of more than 10 indexed EBSD patterns were collected per grain. In the total 1.64 × 1.22 μm area shown in Fig. 3, 94.3% of the grains exhibit {111} orientation (gray) within a 15° misorientation limit relative to ideal {111} orientation. More than 90% of the {111} grains exhibit a misorientation of less than 7.0°. The non-{111} grains (white), consist of 3.1% {100}-textured grains exhibiting a misorientation range of less than 6.0° with respect to ideal {100} and 3.5% randomly oriented grains. The fractions of {111}, {100}, and randomly oriented grains determined from the EBSD texture map are in good agreement with the equivalent volume fractions measured by XRD as described above. Figure 4 is a log plot of the entire misorientation population density distribution with respect to {100} orientation. The misorientation distribution is displayed with respect to {100} orientation since it provides a direct view of the PZT

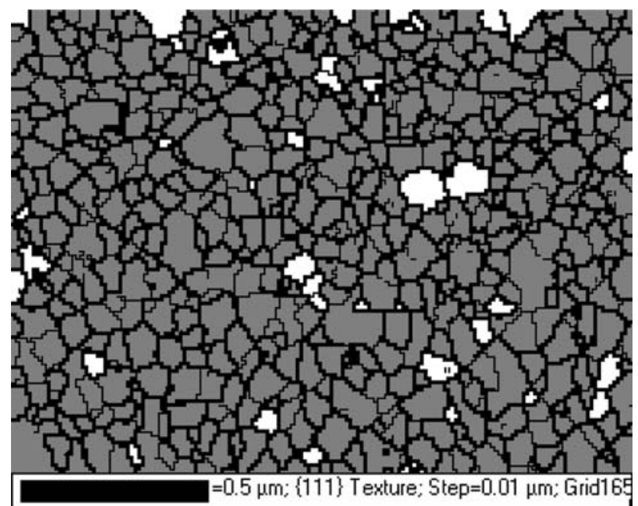

Fig. 3 PZT EBSD map of {111}-textured grains (*gray*) with a misorientation of less than 15° from ideal {111} texture. Non-{111}-textured grains are shown in white. The overlapping grain boundary map shows grain misorientation of 2°–10° (*thin lines*) and greater than 10° (*thick lines*) with a population of 592 grains with an average size of 65 ± 30 nm

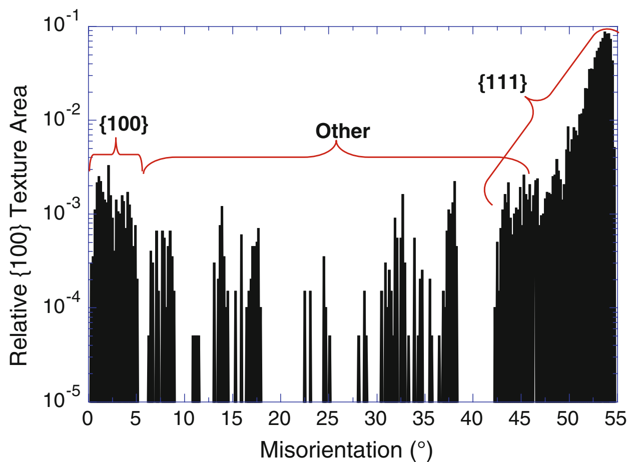

Fig. 4 Relative area distribution of PZT grains as a function of misorientation angle referenced with respect to an ideal {100} texture

ferroelectric polarization density (the ferroelectric polarization lies along the [001] direction) when an electric field is applied along the substrate normal, as is typical for memory device applications. It is observed that the primary, {111}-textured population lies between 40° and 54.74° (the angle between [001] and [111]). A secondary, {100} population occurs between 0° and 6°, and several sparsely populated unidentified or "random" distributions lie between 6° and 40°. Gaps between the distributions indicate that not all "random" orientations grow with equal probability. The average grain size including all orientations is 65 ± 30 nm.

Conclusion

It has been demonstrated that EBSD can map the local orientation of strongly {111}-textured Pt and PZT films with a resolution as high as 5 nm. For the first time, the local texture distributions normal to the substrate surface and corresponding grain size distributions have been quantified for both Pt and PZT films within an area typically used for a single FRAM capacitor. From the large, EBSD-generated texture database collected, it was determined that the PZT grain size, misorientation distribution width, and fraction of non-{111}-textured grains is larger than those observed for the Pt electrode on which PZT is grown; the physical reason for this observation will require additional studies. The observed localized PZT texture distributions indicate that FRAM capacitor areas can be reduced from 2 μm^2 to approximately 0.25 μm^2 before non-{111}-textured grains significantly alter signal margin variability requiring an increase in texture quality.

Acknowledgements The authors would like to thank Prof. Eric Lifshin of the Nanosciences and Nanoengineering Department at the University at Albany—SUNY for providing access to the electron microscopy facilities and Scott Sitzman, HKL Technology, Inc., for helpful discussion on the use of the EBSD analysis software.

References

1. Rodriguez BJ, Gruverman A, Kingon AI, Nemanich RJ, Cross JS (2004) J Appl Phys 95:1958
2. Fox GR, Summerfelt S (2002) Mater Res Soc Proc 721:145
3. Peterson CR, Medendorp NW, Slamovich EB, Bowman KJ (1996) Mat Res Soc Symp Proc 433:297
4. Brooks KG, Reaney IM, Klissurska Huang YH, Bursill L, Setter N (1994) J Mater Res 9:2540
5. Weiss D, Kraft O, Arzt E (2002) J Mater Res 17:1363
6. Muppidi T, Kusama Y, Field DP (2002) Mat Res Soc Symp Proc 721:123
7. Nowell M, Field DP (1998) Mat Res Soc Symp Proc 516:115
8. Nath R, Garcia RE, Blendell JE, Huey BD (2007) JOM 59:17
9. Tai CW, Baba-kishi KZ, Wong KH (2002) Micron 33:581
10. Ernst F, Mulvihill ML, Kienzle O, Rühle M (2001) J Am Ceram Soc 84:1885
11. Fox GR, Suu K (2004) US Patent 6,682,772 (27 January 2004)
12. Chu F, Fox G (2001) Integr Ferroelectr 33:19
13. Chu F, Fox G, Eastep B (2001) US Patent 6,287,637 (11 September 2001)
14. Fox GR (1999) Mat Res Soc Proc 541:529